Appl. Phys. A 72, 463–470 (2001) / Digital Object Identifier (DOI) 10.1007/s003390100579

Applied Physics A
Materials
Science & Processing

High-resolution magnetic imaging by local tunneling magnetoresistance

W. Wulfhekel[1], H.F. Ding[1], W. Lutzke[1], G. Steierl[1], M. Vázquez[2], P. Marín[2], A. Hernando[2], J. Kirschner[1]

[1] Max-Planck-Institut für Mikrostrukturphysik, Weinberg 2, 06120 Halle, Germany
[2] Instituto de Magnetismo Aplicado, Apartado de Correos 155, 28230 Las Rozas, Madrid, Spain

Received: 28 April 2000/Accepted: 15 May 2000/Published online: 7 March 2001 –

Abstract. We give an overview over our recent efforts of high-resolution magnetic imaging using scanning tunneling microscopy with a ferromagnetic tip. Magnetic sensitivity is obtained on the basis of local tunneling magnetoresistance between a soft magnetic tip and the sample. The magnetisation of the tip is switched periodically with a small coil, leading to variations of the tunneling current due to the tunneling magnetoresistance effect. These variations are detected with a lock-in amplifier to separate spin-dependent parts from the topographic parts of the tunneling current such that the topography and the magnetic structure of the sample can be recorded simultaneously. Crucial for this method is to avoid mechanical vibrations of the tip, that may also lead to variations in the tunneling current. Exemplary studies of polycrystalline Ni and the closure domain pattern of Co(0001) are presented, showing high contrast at acquisition times as low as 3 ms/pixel and a lateral resolution of the order of 1 nm. Further it is demonstrated that besides topography and magnetisation, also local information about the magnetic susceptibility can be obtained.

PACS: 75.60.Ch; 75.30.Pd; 75.50.Kj

During the last decades, lateral resolution in magnetic imaging has increased considerably. With surface-sensitive techniques such as scanning electron microscopy with polarisation analysis (SEMPA), spin-polarized low energy electron microscopy (SPLEEM) or magnetic force microscopy (MFM) resolutions of 20–50 nm have been achieved [2–4]. However, it is still a challenge to image magnetic structures down to scales of the exchange length, which is of the order of 10 nm or below in hard magnetic materials. Not only from the fundamental point of view, imaging with a resolution below the exchange length is desirable. Also in commercially available data storage devices, recording density has increased immensely so that bit lengths of 40 nm have been demonstrated, and in the field of patterned or nanostructured media [5–10] and magnetic non-volatile memory cells, magnetic structures on the nanometer scale are aimed at. Unfortunately, the established magnetic imaging techniques start to fail on these length scales and not many experimental facts are known about the structure of domains and domain walls in technically relevant systems on lateral scales of the magnetic exchange length. However, the knowledge about the magnetic structure on these small scales is believed to be crucial for the fundamental understanding of micromagnetism and the controlling of magnetic media and devices in the future. To overcome the obstacles of the established magnetic imaging techniques, the development of the spin-polarized scanning tunneling microscope (Sp-STM) to map the spin structure at surfaces down to the atomic level has been an aim of many studies in the past [11–19]. An instrument with this high a resolution would solve the resolution problem in experimental micromagnetism and would also offer fundamentally new insights into the real space order of antiferromagnets and ferrimagnets at irregular defects such as dislocations, steps or atomic point defects, that are inaccessible to scattering techniques. Two different approaches to obtain sensitivity to the electron spin have been of major importance: first, the use of ferromagnetic tips that lead to a spin-polarized tunneling current and second, GaAs tips with spin-polarized carriers that are created by optical pumping with circulary polarized light. Early attempts in the beginning of the nineties to use ferromagnetic tips and utilise the magneto-tunnel effect [20] were only of limited success. The experiments by Johnson and Clarke [11], who used bulk Ni tips to image the magnetic structure of surfaces in air, were dominated by spurious effects such as magnetostriction of the tip and mechanical vibrations of the tip due to magnetic dipolar forces between tip and sample. Almost at the same time, Wiesendanger et al. [12] claimed to observe spin-polarized vacuum tunneling at room temperature between a ferromagnetic CrO_2 tip and the topological antiferromagnetic Cr(001) surface. However, no separation of topography and spin could be obtained. In the mid-nineties, a more promising approach for magnetic imaging [14–16] using optically pumped GaAs tips and a lock-in technique to separate topographic and magnetic information was established. However, it suffers from a low contrast and an unintended additional optical contrast of limited lateral resolution [21]. To date, no experiments have been published that prove the magnetic origin of the observed domains. Moreover, non-magnetic films are reported to show a considerable signal similar to the domains in magnetic films [16] raising questions about the reliability of this

method. Recently, the first approach to use ferromagnetic tips was revived by different groups [17, 18]. Bode et al. used tips coated with a thin ferromagnet to tunnel into the exchange-split surface state of Gd(0001) [17] and recently also of Fe(001) [22]. A magnetic contrast could be separated from the topography by local tunneling spectroscopy allowing magnetic imaging. However, this method is limited to materials with an exchange-split surface state and requires cryogenic temperatures. In our case, magnetic contrast was obtained by locally measuring the tunneling magnetoresistance between a magnetic tip and the surface of the specimen. By applying an alternating current of frequency f through a small coil wound around the magnetic tips, the longitudinal magnetisation of the tip is switched periodically. The whole volume of the tip is ferromagnetic such that the field of the coil at the back side of the tip switches the magnetisation of the tip, i.e. also the end of the tip, between the two well-known energetically favoured states of opposite magnetisation. For optimal performance the tip material, a metallic glass[1], was chosen to have a low coercivity ($< 50\,\mu$T), vanishing magnetostriction ($< 2 \times 10^{-7}$), low saturation magnetisation (≈ 0.5 T) and low magnetisation losses at high frequencies. These parameters allow a rapid switching of the magnetisation of the tip without mechanical vibrations of the tip due to magnetostriction or magnetisation losses. Furthermore, they minimise the influence of the field of the coil ($\approx 100\,\mu$T) on the sample magnetisation. The frequency $f = 40$–80 kHz was chosen far away from any mechanical resonances of the STM and well above the cut-off frequency of the feedback loop. In this way the variations of the tunnel probability due to the tunneling magnetoresistance effect result in variations of the tunnel current while a constant sample-tip distance is kept. This allows us to separate the spin information from the topographic information. The variations on top of the average tunneling current set by the feed-back loop were detected with a lock-in amplifier. This signal is referred to as spin-signal throughout the remainder of this paper and is given in units of the average tunneling current. The technique offers a high magnetic contrast, fast data acquisition times in the range of ms/pixel and even allows dynamic studies of the local magnetic susceptibility [19].

1 Experiment

The magnetic tips were first prepared in air. Either a tip was cut from a thin commercial foil ($d = 25\,\mu$m) of amorphous material[1] or it was electrochemically etched from specially designed thin wires ($d \approx 100\,\mu$m) of a similar material. The Co-rich amorphous wires are obtained by the in-rotating-water quenching technique [23]. Then the FeCoSiB alloy ingots were molten in a quartz crucible with a 130-μm hole through which the melt was injected into a rotating water bath. This fabrication procedure is responsible for the wire shape and also induces some magnetic anisotropies. The magnetic behaviour of amorphous magnetic wires strongly depends on magnetostriction. Co-rich alloys with adequate additives exhibit vanishing magnetostriction [24] and their hysteresis loops do not show bistability. This kind of wire shows a soft magnetic behaviour associated with a low coercive field and a high initial susceptibility that can be improved by thermal treatments. Annealing below the crystallisation temperature causes microscopic rearrangements that give rise to a reduction in the internal stresses coming from the fabrication process [25]. Modifications in the magnetostriction constant are produced mainly by these topological changes. For both types of tips, cut from foil or etched from a wire, only the very end of the tunneling tip was made out of the magnetic material to minimise the mechanical vibrations caused by the magnetic forces between tip and the magnetising coil. Using a conducting glue, the magnetic part of the tip was fixed to a tip shaft ($d \approx 500\,\mu$m). Around the shaft of the tip, a magnetic coil (inner diameter $\approx 600\,\mu$m) was wound and was mechanically fixed to the shaft by insulating glue to avoid vibrations. The coil is used to switch the longitudinal magnetisation of the tip. In this way sensitivity for the perpendicular magnetic component of the sample is obtained. However, for the tips cut from foil, we were in poor control of the shape of the mesoscopic end of the tip. A somewhat tilted end of the tip can lead to an additional sensitivity to the in-plane magnetic components. However, for etched tips, the magnetisation has to lie along the tip axis for micromagnetic reasons.

The STM experiments were performed in an ultrahigh vacuum chamber system ($p = 5 \times 10^{-11}$ mbar) equipped with an Auger electron spectrometer (AES), a differentially pumped sputter gun, a low-energy electron diffractometer (LEED), a modified commercially available room temperature STM [26] and a magnet to magnetise samples in the STM stage. Care was taken in the STM design to avoid magnetic parts in the sample stage and scanning unit to allow the operation of the STM in an applied magnetic field. Further, the chamber system is equipped with a two-stage load-lock to transfer samples and tips into and out of the vacuum without breaking the vacuum. The pressure in the main chamber is kept at 2×10^{-10} mbar during the transfer of samples and tips and it returns to its base value immediately after the transfer. After transferring new tips to the STM the magnetic tips were cleaned in situ by sputtering with 1-keV Ar^+ ions to remove the native oxide at the apex of the tip. Samples were cleaned by cycles of argon sputtering (1 keV) and annealing until no traces of contaminations could be found in AES spectra and LEED images showed a sharp diffraction pattern with a low background intensity. The Cu(001) and Cr(001) crystals as well as the polycrystalline Ni block were annealed up to 800 K, whereas the Co(0001) crystal was heated only to 570 K to stay below the well known hcp–fcc phase transition of Co at ≈ 690 K. Due to the limited annealing temperature for Co(0001), the surface remained with a low concentration of small defects – either sputter defects such as adatom or vacancy islands or local fcc or misoriented hcp areas, as has been observed also by others [27]. After sample and tip preparation, tunneling images of the topography as well as the magnetisation were recorded at room temperature.

2 Results and discussion

2.1 Initial tests for magnetisation reversal and residual vibrations of the tip

First, we investigated whether the magnetisation of the tip can be switched with low fields and tested whether imaging is

[1] Good results were obtained with CoFeNiSiB amorphous foils (Vitrovac) from Vacuumschmelze Hanau

possible during switching. To check, for magnetisation reversal of the tip, we used an additional pick-up coil mounted at the end of the tip and recorded the induction as a function of the field of the exciting coil. For fields below $\approx 40\,\mu$T, induction was negligible, indicating that the field was insufficient to switch the tip magnetisation. When the exciting field exceeded $\approx 50\,\mu$T we observed a steep increase of the induction indicating the switching of the tip. Upon further increase of the exciting field, only a small increase of the induction was observed. This agrees with the complete switching of the tip magnetisation above a threshold field of around $50\,\mu$T in accord with the hysteresis of the material. The slight increase upon further increase of the field is consistent with direct induction between the two coils. A priori, it was not clear if stable tunneling could be obtained while the magnetisation of the tip is rapidly switched. Many effects such as induction into the tunneling circuit and vibrations of the tip can prevent one imaging the surface. To check for these effects, we performed test measurements of the Sp-STM set-up on nonmagnetic samples in UHV. Figure 1a displays the topography of a Cu(001) crystal as obtained with a tip, which was cut from foil and cleaned in situ, while exposing it to an alternating field of ≈ 1 mT. Terraces separated by atomic steps are clearly visible and the lateral resolution of the tip is sufficiently good. Obviously induction into the tunneling circuit is small enough to allow imaging, and vibrations due to magnetic forces or magnetostriction are small enough to get stable STM images[2]. In the spin signal obtained from the lock-in amplifier, however, one observes some contrast at the step edges (see Fig. 1b). This cross-talk from the topography is of the order of 0.3% of the tunneling current and is due to small mechanical vibrations of the tip. These vibrations can be avoided, when the exciting field is reduced by one order of magnitude (see Fig. 1c and d). The spin signal in this case is zero and does not show any cross-talk from the topography while the magnetisation of the tip is still switched. Hence, vibrations due to magnetostriction and magnetic forces between the coil and the tip can be excluded down to the sensitivity of the lock-in detection of $< 0.1\%$ of the tunneling current. Taking the well-known dependence of the tunneling current on the distance [28] with a tunneling voltage of 0.2 V, a tunneling barrier height of 3 V and a tunneling current of 1 nA, one can estimate the vibration in the narrow frequency band around the modulation frequency. The lock-in signal corresponds to distance changes between tip and sample of less than 5×10^{-4} Å, i.e. mechanical vibrations due to magnetostriction of the tip or due to magnetic interaction between the tip and the coil can safely be neglected.

[2] Some vibrations visible as ripples in the topography are not related to the switching of the tip but to insufficient damping of vibrations of the building caused by the construction of a new road in front of the institute

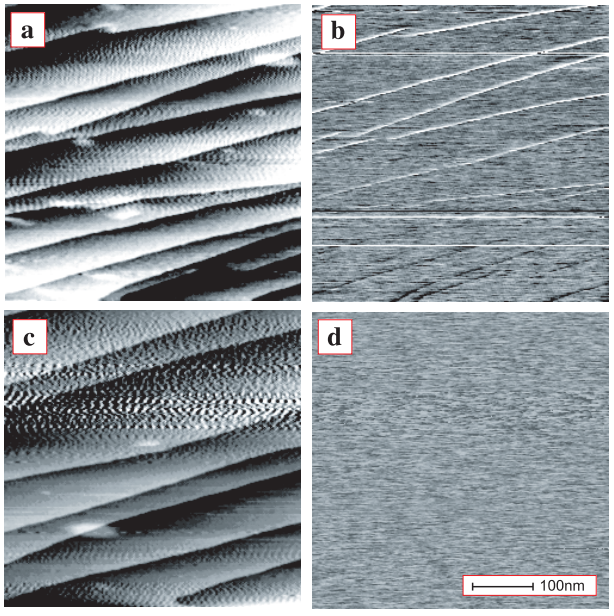

Fig. 1a–d. STM scans of the topography (**a**,**c**) and the spin signal (**b**,**d**) of the same areas (**a**,**b** and **c**,**d**) of Cu(001). During scanning an alternating magnetic field of 20 kHz was created by the coil around the tip. The field was set to 1.1 mT (**a**,**b**) and 100 μT (**c**,**d**). For the higher field, mechanical vibrations of the tip are observed causing a cross-talk from the topography into the spin signal. Both spin images (**b**,**d**) are normalised to a black and white contrast corresponding to 0.3% of the tunneling current

2.2 First magnetic tests: polycrystalline Ni

After the initial test on a non-magnetic substrate, we intended to check whether a non-vanishing signal can be obtained on a ferromagnetic surface. As a test surface we chose a polished but polycrystalline Ni disk. On large, several μm^2 scans of the Ni surface, strong contrasts can be found in the spin-signal as displayed in Fig. 2a. The image of the spin-signal shows two regions, i.e. domains, with different intensity, separated by a fine, bright line, i.e. a domain wall. The observed features in the spin-signal are not related to the topography as can be seen by comparing the topography of Fig. 2b with the spin-signal of the very same area (white box in Fig. 2a). This excludes that the observed features are caused by a cross-talk from the topography. In agreement with the complete switching of the tip magnetisation, the observed domains in the spin-signal disappear suddenly when the size of the exciting field is lowered below $\approx 40\,\mu$T and reappear for fields

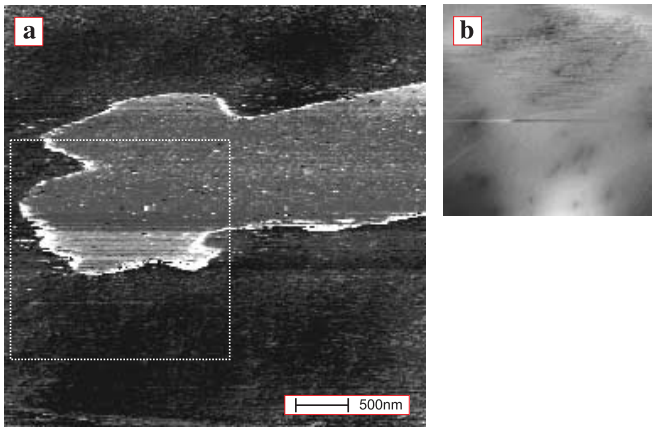

Fig. 2a,b. Sp-STM scans of the spin structure of a polished polycristalline Ni surface (**a**). To show that the observed spin contrast is unrelated to the morphology, the topography (**b**) and the spin signal (*white box* in **a**) of the very same area were recorded. Measuring parameters: $U = 130$ mV, $I = 1$ nA, $f = 82$ kHz, $H = 100\,\mu$T. The contrast in the spin signal is 0.5% of the tunneling current. The peak to peak roughness of the topography corresponding to full black white contrast is 3 nm

above $\approx 50\,\mu$T. Upon further increase of the field the observed contrast in the domain images does not rise further. This is consistent with the switching behaviour of the tip and points at a purely magnetic contrast. The width of the domain walls observed by us on polycrystalline Ni is between 100 and 150 nm and hence in qualitative agreement with calculated wall widths of 85–200 nm depending on the wall type and the crystal orientation of Ni [29]. Also this points at a magnetic contrast. Moreover, the domains in the spin-signal are changing on the time scale of hours during repeated scanning, which rules out that the contrast is caused by some other, static characteristic such as compositional, structural or orientational variations of the sample surface. However, to strictly prove that we indeed have magnetic contrast, we chose a better defined surface than polycrystalline Ni for our further studies.

2.3 The closure domain structure of Co(0001)

Hcp cobalt is magnetically much harder than Ni and displays a strong uniaxial magnetocrystalline anisotropy with an easy direction along the *c* axis, i.e. perpendicular to the selected (0001) surface. Due to the minimisation of the stray field energy and the net magnetic flux exiting the surface, the single domain state is unstable and splits up into a Lifshitz closure domain pattern [30]. Since for Co the magnetic anisotropy and the dipolar energy are of the same order of magnitude [29], no simple closure domain structure occurs on the (0001) surface. Instead, a complex, micron-sized structure is observed [27, 31, 32], where the magnetisation of most areas of the surface of the closure domains is strongly rotated away from the surface normal as observed for example with SEMPA [27]. As a consequence of this, the surface splits up into domains with mainly in-plane magnetisation with only a small out-of-plane component. This leads to a similarly shaped but somewhat washed out domain pattern in the perpendicular component with domains with small alternating up and down perpendicular components. We use Sp-STM to study this complex structure with high resolution. Figure 3a displays the topography of the Co(0001) surface on a large scale. Due to a slight and practically unavoidable miscut of the sample, steps are present on the surface that bunch during annealing to form step bunches 1–2 nm high, separated by flat terraces ≈ 500 nm wide. This leads to some roughness of the surface. Keeping in mind that the scans extend over several μm, i.e. are rather large for a high-resolution technique such as STM, the observed roughness of a few nm still corresponds to a very flat surface. Figure 3b shows the magnetisation of the very same area of the sample, as seen with the spin-polarized STM using a tip cut from foil. The expected closure domain pattern with domains of the order of 500 nm is observed in agreement with SEMPA experiments [27, 30]. However, the observed contrast is most likely not completely due to the perpendicular component of the sample magnetisation. A certain in-plane sensitivity cannot be excluded for tips cut from foil because of our poor control of the tip shape. Many of the closure domains are pinned at the step bunches giving alternating magnetisation on adjacent flat regions of the sample. The influence of the topography on the local arrangements of closure domains is not unknown and has been reported for structures on larger scales [30].

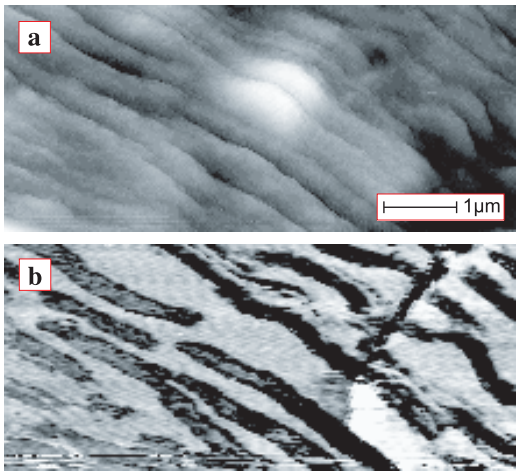

Fig. 3a,b. Sp-STM scans of the topography (**a**) and the spin structure (**b**) of the very same area on a Co(0001) surface. Measuring parameters: $U = 200$ mV, $I = 1$ nA, $f = 82$ kHz, $H = 100\,\mu$T. Height variations in **a**: 4 nm. Contrast in the spin signal in **b**: 3.6% of the tunneling current

However, there are also domains that are not correlated to the morphology (see upper right corner of Fig. 3b). The contrast in the magnetic image, i.e. the tunneling magnetoresistance, is mostly smaller than that corresponding to tunneling experiments [33, 34]. This is due to the fact that the majority of surface domains on Co(0001) shows only a small perpendicular component [27, 31] giving a small projection on the axis of magnetisation of the tip.

The observation of a contrast in the spin channel, even if the expected domain structure is seen, is no rigorous proof for a magnetic origin of the signal. To exclude all other origins, we did a proper magnetic experiment. We carried out dynamic measurements and studied the influence of a magnetic field on the features in the spin-signal. Unlike on polycrystalline Ni, the observed features on Co(0001) show only minor changes even after extended scanning of the same area over hours. When applying a short pulse of a homogeneous magnetic field of the order of 5 mT perpendicular to the sample surface as indicated by the arrows in Fig. 4, the observed domain wall can be moved a couple of μm during scanning (see Fig. 4a) while no movement is observed in the topographic image (see Fig. 4b). This unambiguously proves the

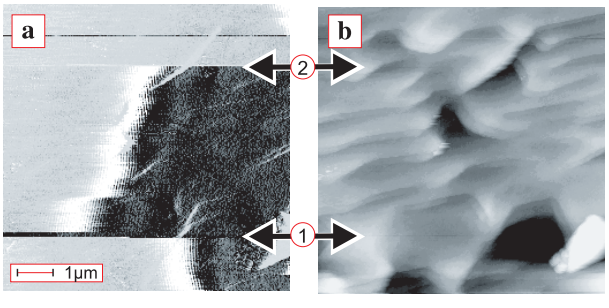

Fig. 4a,b. STM image of the domain structure (**a**) and topography (**b**) of the same area of the surface of Co(0001). When applying external magnetic field pulses of 5 mT during scanning (indicated by the *arrows*), the domain wall can be moved to the left (1) or right (2), depending on the direction of the field. No movement is observed in the topography. Measuring parameters: $U = 200$ mV, $I = 1$ nA, $f = 41$ kHz, $H = 100\,\mu$T

magnetic origin of the spin-signal. The observed structures are indeed magnetic domains and domain walls on the surface. Additionally, this illustrates that spin-polarized STM can be used for high-resolution studies of domain wall motion dynamically during scanning. However, the magnetic field used to move the domain wall is much larger than the alternating field used to switch the magnetisation of the tip and the tip magnetisation is fixed for the duration of the pulse. Thus, during the short magnetic pulse the lock-in signal is lost and neither domain walls nor domains are observed in the parts of Fig. 4a that are indicated by the arrows.

2.4 Ultra-narrow domain walls

Spin-polarized STM using a ferromagnetic tip poses some constraints on the shape of the tunneling tip. To obtain good resolution the very end of the tip has to be atomically sharp. This also determines the magnetic resolution. When imaging domain walls or soft magnetic materials, however, the stray field of the magnetic tip cannot be neglected, since it might influence the magnetic structures under investigation. To minimise this influence and to obtain the highest magnetic resolution, the flux exciting the end of the tip has to be minimised. This is done by producing very sharp magnetic tips by slow etching. The end of a tip can be seen in Fig. 5. It was electrochemically etched from a 100-μm magnetic wire within 30 min, i.e. etching was very slow. This slow etching results in very sharp and elongated tips. Usually, one would not choose such tips for STM studies, because they have a tendency to become unstable during scanning. For Sp-STM, however, these tips give best results for the magnetic resolution since the magnetostatic interaction between tip and sample is minimised. Additionally, due to the extreme shape of the etched tips, their magnetisation lies along the tip axis and hence, with etched tips, we get sensitivity only for the perpendicular magnetic component of the sample. In accord with this, on large-scale images we observe the complex and dendritic perpendicular domain pattern as seen before with SEMPA [27].

Figure 6a displays an STM image of the topography of the Co(0001) surface with two atomic terraces and some point defects. Figure 6b shows the perpendicular magnetisation component of the same area of the sample, as seen with the Sp-STM. The displayed area was selected from large

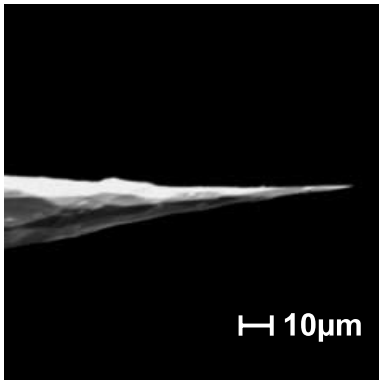

Fig. 5. Scanning electron microscopy image of the end of magnetic tip etched from a 100-μm amorphous wire

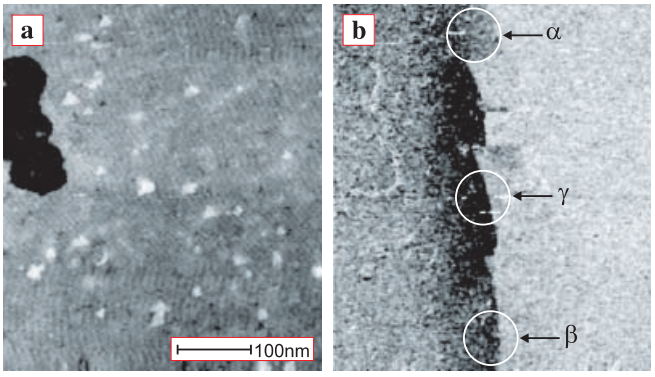

Fig. 6a,b. STM images of the topography (**a**) and the perpendicular component of the magnetic domain structure (**b**) of the same area of Co(0001). Measuring parameters: $U = 200\,\mathrm{mV}$, $I = 1\,\mathrm{nA}$, $f = 41\,\mathrm{kHz}$, $H = 70\,\mu\mathrm{T}$

scans of the closure domain pattern so that it contains one domain wall close to a point in the domain pattern, where several domains meet. These special points are regularly found with Sp-STM at the end of the dendritic structures and have also been observed with SEMPA [27]. The domain wall in the magnetic images (see Fig. 6b) is not correlated with the topography or pinned at a topographic defect (compare Fig. 6a). Only at some step edges, for example at the lower terrace in the left part of Fig. 6b, a weak cross-talk of the topography to the magnetic image is present. By applying a magnetic field and observing the wall movement with respect to the topography, it was checked that the observed structure indeed is a magnetic domain wall. The domain wall separates the left side of Fig. 6b with a perpendicular magnetisation component that points into the surface from the right side where the perpendicular component points out of the surface. Interestingly, the wall shows some structure along its axis. It splits up into segments of different wall width. In section α a gradual transition between the two domains is observed, whereas in section β it is considerably sharper. In section γ the transition seems to be abrupt on the scale of the image. The different, rather straight sections are separated by kinks in the domain wall.

To quantify the differences in wall width, we recorded line scans across the different sections of the wall. Figure 7 displays the measured wall profiles obtained by averaging 20 line scans across each section of the wall. The error bars represent the statistical error from averaging. Note that the line scans, especially across the narrow sections of the wall, have been taken with higher magnification than Fig. 6 to avoid lateral sampling noise. Additionally, the scanning speed was set such that neighbouring data points are separated by more than two times the integration time τ of the lock-in amplifier to ensure that the data points are statistically independent and the wall profile is recorded correctly. From the figure it is obvious that the wall width of the different sections varies by more than one order of magnitude (note the different scales on the x axes). To estimate the wall width $w = 2\delta$, we fit the profiles with the standard wall profile for uniaxial systems [29]:

$$m_z = \tanh\left(\frac{x}{\delta}\right) , \tag{1}$$

resulting in the following width for the different sections: α: $w = 45 \pm 8\,\mathrm{nm}$, β: $w = 8.7 \pm 3.2\,\mathrm{nm}$, γ: $w = 1.1 \pm 0.3\,\mathrm{nm}$.

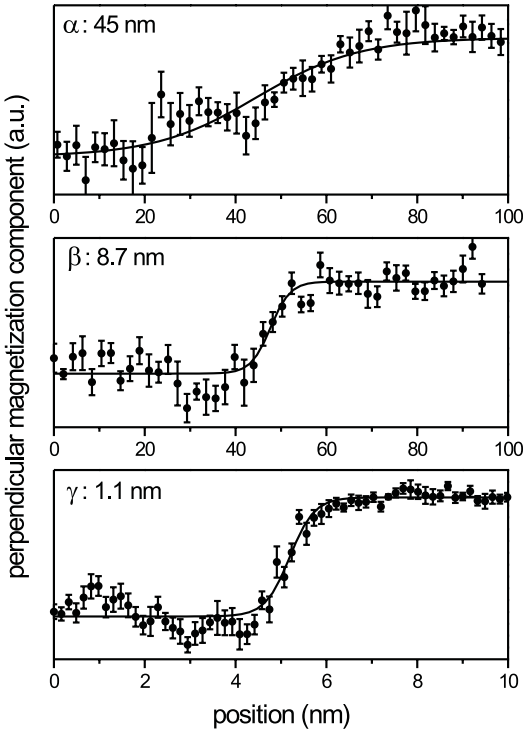

Fig. 7. Averaged line profiles across different sections of the domain wall as indicated in Fig. 6b including the statistical errors and fits with the standard wall profile (*solid lines*). Fitted wall widths are given in the figure. Note the different scale of the x axis of the bottom line profile

The wall width of section α is broader than the width of a bulk 180° Bloch domain wall of ≈ 16 nm [29]. The broadening of domain walls at the surface is well known and has also been seen for this particular surface of Co [27]. However, sections β and especially γ are much narrower than the bulk domain wall. At first glance, section γ seems to be unphysically narrow. To check for instrumental reasons for the observation of such narrow walls, we make the following considerations. One possible mechanism that might lead to seemingly ultra-narrow walls could be a non-linear response of the instrument to the perpendicular component of the magnetisation, for example a response like a step function. The magneto-tunnel effect, however, is a linear effect with the projection of the magnetisation of the sample onto that of the tip [35]. Hence, the observed signal should be proportional to the perpendicular component of the sample magnetisation. Additionally, a step-shaped response function should narrow all the domain walls, while we observe walls of largely different width with continuous transitions in the wall profiles even in a single scan of the surface together with the ultra-narrow domain walls (see Fig. 6b and Fig. 7 profile α). This rules out that we have a transfer function that artificially sharpens the walls.

An alternative explanation could be that we pick up the domain wall with the magnetic tip and drag it along during scanning until it snaps off. In that case a sharp transition would be observed at the point of snapping off. To test for this mechanism, we recorded the wall while scanning from the right to the left and in the opposite direction (see Fig. 8). If the wall is dragged along and snaps off, an opposite displacement of the wall for scanning in the two directions should be seen. However, the domain wall appears at exactly the same

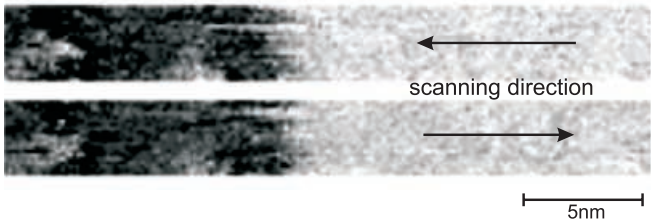

Fig. 8. Detailed Sp-STM images of the perpendicular component of the magnetisation scanning across section γ from the right to the left (*top*) from the left to the right (*bottom*) taken simultaneously at the same area of the Co(0001) sample. $U = 200$ mV, $I = 1$ nA, $f = 41$ kHz, $H = 70$ μT

position for both directions (see Fig. 8), ruling out any significant dragging. Hence, we have to consider that the observed ultra-narrow domain walls are real. This, at first sight, might contradict common knowledge about domain walls. The wall in segment γ is more than one order of magnitude narrower than a Bloch wall in bulk Co. This is very surprising, since the walls observed on the surface originate from domains that penetrate into the bulk of the crystal. Also geometrical constrains can be ruled out, that in some cases lead to a narrow wall [36].

To understand the origin of the narrow walls, we focus on the complex nature of the closure domain pattern of Co(0001). As SEMPA experiments show [27], the magnetisation splits up into domains separated by domain walls across which the in-plane component rotates by the possible angles of 0, 60, 120 or 180°. Due to the competition between stray field energy and magnetocrystalline anisotropy, these in-plane domains have a small out-of-plane component resulting in a domain pattern in the perpendicular component with domains with small up and down perpendicular components. When measuring the contrast across the domain wall of Fig. 6b with Sp-STM and comparing it to the maximum contrast observed in large scale scans one realises that the wall displays only ≈ 18% of the total contrast roughly in the middle between maximal and minimal values. Hence, we see with Sp-STM, that the magnetisation mainly lies in-plane with only a small component along the surface normal in agreement with earlier measurements [27]. Under the assumption that the minimum and maximum values observed in large Sp-STM scans correspond to fully perpendicular up and down magnetisation, one can calculate the angle of magnetisation from the surface plane on the two sides of the ultra-narrow domain wall to ≈ ±10°. Also analytically, when taking the recently reviewed tilted closure domain model by Hubert et al. [31] with the anisotropy values for Co(0001), one obtains an angle of ±10° for the magnetisation with respect to the surface plane. This is in excellent agreement with our measurements. This leads to the following model. Going from one surface domain to the next, the out-of-plane angle changes by 0 or ±20° while the in-plane angle changes by 0 or a multiple of 60°. The width of the simplest domain wall, i.e. the wall with no change of the in-plane angle but a reversal of the small out-of-plane component, can be calculated straightforwardly. Following the standard procedure for the calculation of domain wall widths by minimising the sum of exchange and the anisotropy energy [29, 37], one obtains a width of $w = 1.5$ nm in fairly good agreement with the experimentally observed width of section γ. This shows that the ultra-narrow domain walls are real, and are not at vari-

ance with the laws of micromagnetism. The magnetostatic energy has been neglected in this calculation. However, the surface charge density is small due to the shallow angle of the magnetisation. Additionally, surface anisotropies at the Co–vacuum interface might reduce the wall width. A similar width can also be estimated by a rule of thumb argument. A 180° domain wall has a width of ≈ 16 nm [29]. A 20° domain wall should have a width of a fraction of 20/180 of this. The observed ultra-narrow walls can be explained by a domain wall where the magnetisation direction is changed by only ≈ 20°. When, however, not only the out-of-plane but also the in-plane angle changes by for example 60° or 120° across the domain wall, the wall width is considerably wider due to the larger angle the magnetisation has to be rotated. An analytical calculation for the profile of these walls is not possible following the simple standard methods. However a lower limit for the wall width can be estimated by a rule of thumb argument to ≈ 5 nm for a 60° and ≈ 11 nm for a 120° wall.

With the etched tips we achieve sensitivity for only the perpendicular component. That means within the simple domain model, that walls which only display a rotation in-plane are invisible and all walls that have out-of-plane changes have identical contrast. At the special points where the ultra-narrow domain walls are observed, several small domains touch. These points have been observed also with SEMPA [27]. Hence, different types of domain walls are present at these points. This explains our Sp-STM observations. The different sections of the visible domain wall correspond to domain walls with different in-plane rotation, possibly 0° for section γ, 60° for section β and 120° for section α, while the domain walls where only the in-plane angle changes are not visible within the noise level. However, the points where the in-plane domain walls meet the visible out-of-plane wall, the out-of-plane wall displays kinks. A detailed image of low noise level of such a kink is shown in Fig. 9, displaying a third, triangular domain of very weak contrast in the upper part. The lower part of the domain wall belongs to the ultra-narrow section γ of Fig. 6b. In the uppermost part, the wall widens. This supports our assumption, that the angle of rotation in the film plane across the different sections of the domain wall is different leading to different wall widths. The finding of sharp domain walls on the surface of Co(0001) also gives some experimental evidence for the theoretical predictions of Hubert and Rave that sharp wall-like transitions can be formed at the surface of a closure domain pattern [38], especially when higher order in- or out-of-plane anisotropy terms are present as is the case for Co(0001). Why the sharp walls are only observed close to special points in the closure domain pattern remains an open question. Possibly only at these singular points the magnetic flux is compensated is such a way, that the total anisotropy term becomes stationary [31, 38].

The observation of the ultra-narrow sections in the domain walls of the closure domain pattern of Co(0001) is not only a very surprising micromagnetic result. It also gives us an estimate for the lateral resolution of our instrument of about 1 nm. This high a resolution and as a consequence detailed wall profiles opens up a new view to experimental micromagnetism and illustrates the potential of Sp-STM.

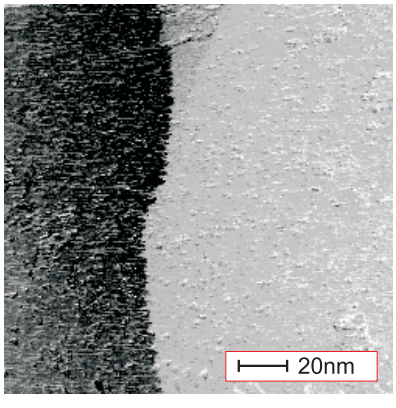

Fig. 9. Sp-STM image of a detail of the magnetic structure of an ultra-narrow section of a domain wall close to a kink. Note a triangular third domain at the top of the image. Measuring parameters: $U = 200$ mV, $I = 1$ nA, $f = 41$ kHz, $H = 70$ μT

2.5 Magnetic susceptibility

In contrast to the previous section, where we minimised the influence of the tip magnetisation on the sample by using a sharp tip, we now want to have a measurable influence. Freshly prepared tips that are also sharp on the mesoscopic scale produce a rather localised stray field; the domain walls of hard magnetic materials are not effected and are resolved with high resolution as in Fig. 6. When, however, a tip is used that is dull from the beginning by optical inspection or is dull due to several severe tip crashes, domain walls are smeared out as in Fig. 10a. This is due to a periodic domain wall movement induced by the alternating field of the tip. The walls rapidly vibrate with the magnetisation frequency f, such that the resolution is limited to ≈ 1000 nm (see Fig. 10a), while the topographic resolution is still good. This magnetic interaction between tip and sample is not necessarily unwanted, but can also be used to locally measure the magnetic susceptibility of a sample. Since the sample magnetisation cannot follow instantaneously the stray field of the tip, a phase difference between the magnetisation of the tip and the sample exists and due to the nonlinearity of the magnetisation process, higher harmonics in the tunneling current are produced. These can be detected with a second lock-in amplifier simultaneous with the spin signal. This mechanism may be used to obtain domain wall contrast as shown in Fig. 10b ($2f$-signal). From the observed width of the susceptibility signal around

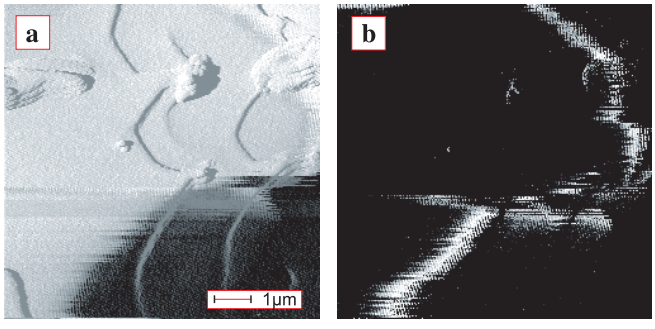

Fig. 10a,b. STM images of the magnetic domain structure (**a**) and magnetic susceptibility (**b**) of the same area on Co(0001). Measuring parameters: $U = 200$ mV, $I = 0.5$ nA, $f = 41$ kHz, $H = 70$ μT

the wall and the switching frequency f, a local domain wall speed of $\approx 10\,\mathrm{cm/s}$ can be estimated. Hence, not only static measurements of the sample magnetisation can be carried out with Sp-STM, but the intrinsic stray field of dull tips may be used to carry out dynamic studies while recording magnetisation and topography at the same time. This technique in combination with higher switching frequencies might even allow local studies of the switching behaviour of individual magnetic nanostructures. Note that for the sharp tips used in the previous section, no measurable susceptibility signal was detected in the domain walls, showing that the magnetostatic interaction in that case can be suppressed efficiently.

3 Summary

We have shown that Sp-STM using ferromagnetic tips is a simple and powerful method to study the surface magnetisation with excellent resolution and high contrast. Our method allows operation at room temperature with data acquisition rates of the order of ms/pixel and allows the separation of spin information from the topography. The demonstrated lateral resolution in the spin channel of down to 1 nm is only limited by the sharpness of the available magnetic structures. By dynamic studies in an applied field, we have proven that the observed contrast is indeed a magnetic one. Further we have shown that besides quantitative static information about the magnetisation, also dynamic studies of the magnetic susceptibility can be carried out. This allows us to study wall mobilities and the switching behaviour of magnetic structures and enables one to quantify the magnetostatic tip-sample interaction.

Acknowledgements. The authors acknowledge discussions with H.P. Oepen, H. Itoh, J. Shen and O. Fruchart.

References

1. H.P. Oepen, J. Kirschner: Scanning Microsc. **5**, 1 (1991)
2. H. Matsuyama, K. Koike: J. Electron Microsc. **43**, 157 (1994)
3. T. Duden, E. Bauer: Phys. Rev. B **59**, 468 (1999)
4. L. Abelmann, S. Porthun, M. Haast, C. Lodder, A. Moser, M.E. Best, P.J.A. van Schendel, B. Stiefel, H.J. Hug, G.P. Heydon, A. Farley, S.R. Hoon, T. Pfaffelhuber, R. Proksch, K.J. Babcock: J. Magn. Magn. Mater. **190**, 135 (1998)
5. W. Wernersdorf, E. Bonet Orozco, K. Hasselbach, A. Benoit, B. Barbara, N. Demoncy, A. Loiseau, H. Pascard, D. Mailly: Phys. Rev. Lett. **78**, 1791 (1997)
6. C. Chappert, H. Bernas, J. Ferré, V. Kottler, J.P. Jamet, Y. Chen, E. Cambril, T. Devolder, F. Rousseaux, V. Mathet, H. Launois: Science **280**, 1919 (1998)
7. T. Aign, P. Meyer, S. Lemerle, J.P. Jamet, J. Ferré, V. Mathet, C. Chappert, J. Gierak, C. Vieu, F. Rousseaux, H. Launois, H. Bernas: Phys. Rev. Lett. **81**, 5656 (1998)
8. H. Brune, M. Giovannini, K. Bromann, K. Kern: Nature **394**, 451 (1998)
9. O. Fruchart, M. Klaua, J. Barthel, J. Kirschner: Phys. Rev. Lett. **83**, 2769 (1999)
10. W. Wulfhekel, F. Zavaliche, F. Porrati, H.P. Oepen, J. Kirschner: Europhys. Lett. **49**, 651 (2000)
11. M. Johnson, J. Clarke: J. Appl. Phys. **67**, 6141 (1990)
12. R. Wiesendanger, H.J. Güntherodt, G. Güntherodt, R.J. Gambino, R. Ruf: Phys. Rev. Lett. **65**, 247 (1990)
13. S.F. Alvarado, P. Renaud: Phys. Rev. Lett. **68**, 1387 (1992)
14. M.W.J. Prins, R. Jansen, H. van Kempen: Phys. Rev. B **53**, 8105 (1996)
15. Y. Suzuki, W. Nabhan, K. Tanaka: Appl. Phys. Lett. **71**, 3153 (1997)
16. Y. Suzuki, W. Nabhan, R. Shinohara, K. Yamaguchi, T. Katayama: J. Magn. Magn. Mater. **198-199**, 540 (1999)
17. M. Bode, M. Getzlaff, R. Wiesendanger: Phys. Rev. Lett. **81**, 4256 (1998)
18. W. Wulfhekel, J. Kirschner: Appl. Phys. Lett. **75**, 1944 (1999)
19. W. Wulfhekel, H.F. Ding, J. Kirschner: J. Appl. Phys. **87**, 6475 (2000)
20. M. Julliere: Phys. Lett. **54A**, 225 (1975)
21. M.W.J. Prins, R.H.M. Groeneveld, D.L. Abraham, H. van Kempen, H.W. van Kersteren: Appl. Phys. Lett. **66**, 1141 (1995)
22. O. Pietzsch, A. Kubetzka, M. Bode, R. Wiesendanger: Phys. Rev. Lett. **84**, 5212 (2000)
23. I. Ohnaka: Intl. J. Rapid Solidfn. **1**, 219 (1984-85)
24. M. Vázquez, J. González, A. Hernando: J. Magn. Magn. Mater. **53** 323 (1986)
25. C. Gómez-Polo, M. Vázquez: J. Magn. Magn. Mater. **118**, 86 (1992)
26. Micro-STM, Omicron Vakuumphysik GmbH, Idsteiner Str. 78, 65232 Taunusstein, Germany
27. J. Unguris, M.R. Scheinfein, R.C. Celotta, D.T. Pierce: Appl. Phys. Lett. **55**, 2553 (1989)
28. See for example Y. Kuk: In *Scanning Tunneling Microscopy I*, ed. by H.J. Güntherodt, R. Wiesendanger (Springer, Berlin, Heidelberg 1992)
29. E. Kneller: In *Ferromagnetismus* (Springer, Berlin, Heidelberg 1962)
30. D. Craik, R.S. Tebble: In *Ferromagnetism and ferromagnetic domains* ed. by E.P. Wohlfahrt (North-Holland, Amsterdam 1965) p. 119
31. A. Hubert, R. Schäfer: In *Magnetic Domains* (Springer, Berlin, Heidelberg 1998)
32. W. Rave, E. Zueco, R. Schäfer, A. Hubert: J. Magn. Magn. Mater. **177-181**, 1474 (1998)
33. Y. Lu, X.W. Li, G. Xiao, R.A. Altman, W.J. Gallagher, A. Marley, K. Roche, S. Parkin: J. Appl. Phys. **83**, 6515 (1998)
34. J.S. Moodera, J. Nowak, R.J.M. van de Veerdonk: Phys. Rev. Lett. **80**, 2941 (1998)
35. J.C. Slonczewski: Phys. Rev. B **39**, 6995 (1989)
36. P. Bruno: Phys. Rev. Lett. **83**, 2425 (1999)
37. A. Aharoni: In *Introduction to the Theory of Ferromagnetism* (Oxford University Press, New York 1996)
38. A. Hubert, W. Rave: J. Magn. Magn. Mater. **196-197**, 325 (1999)